Discrete-Time Anti-windup Compensation for Synchrotron Electron Beam Controllers with Rate Constrained Actuators ⋆

Sandira Gayadeen [a], Stephen R. Duncan [b]

[a] *Diamond Light Source, Harwell Science and Innovation Campus, Didcot, OX11 0DE, UK*

[b] *Department of Engineering Science, University of Oxford, Parks Road, Oxford, OX1 3PJ, UK*

Abstract

By accelerating electrons to relativistic speeds, synchrotrons generate extremely intense and narrow beams of electromagnetic light that are used for academic research and commercial development across a range of scientific disciplines. In order to achieve optimum performance, the stability of the electron beam is a crucial parameter for synchrotrons and is achieved by a beam stabilisation system that is used to control the location of the electron beam and minimise any instability of the electron beam caused by external disturbances. Slew rate limits are common nonlinearities encountered with the actuators in synchrotron feedback systems which can impose significant limitations on the robustness and the performance of the control system. This paper describes an Internal Model Control (IMC) based anti-windup synthesis using an algebraic Riccati equation for a discrete-time control system to compensate against the performance deterioration in the presence of rate constraints. An Integral Quadratic Constraint (IQC) framework is used to analyse the robust stability of the anti-windup augmented closed loop system in the presence of norm-bounded uncertainty. The anti-windup augmented controller is implemented at Diamond Light Source, the UK's national synchrotron facility and improvements in robustness and performance were achieved with respect to the use of no anti-windup compensation.

Key words: Anti-windup, Internal Model Control (IMC)

1 Introduction

Diamond Light Source is the UK's national synchrotron facility which is capable of producing light of exceptional brightness and intensity that is used in a wide range of experimental techniques to probe atomic structure. At Diamond Light Source electrons are accelerated through a linear accelerator (linac) and a booster synchrotron until they reach an energy of 3GeV. The electrons are then injected into a circular storage ring of circumference 561m where they circulate for several hours at constant energy. A combination of large, strong magnets deflect the electrons around the circular orbit, causing them to lose energy in the form of extremely intense and narrow beams of electromagnetic light referred to as 'synchrotron light'. Photon beamlines are placed tangentially to the storage ring to guide the narrow beams of light to experimental stations, where the light is used in a range of experiments from the design of drugs to treat viruses, to the development of non-destructive techniques in palaeontology and in the development and characterisation of novel materials for engineering applications.

In order for synchrotron light sources to produce high brilliance photon beams, the emittance (i.e. the spread of photons) must be reduced both horizontally and vertically. The vertical *electron beam* size defines the emittance of the *photon beam* and thereby to reduce the emittance of the photon beam, tight requirements are imposed on the electron beam size. Although the size and shape of the electron beam is maintained by the magnetic fields within the storage ring, the beam is subjected to disturbances from environmental effects that are coupled through the girders that support the magnets. This causes the size of the electron beam to

⋆ Some material in this paper was presented at the 2013 European Control Conference, July 17-19, Zürich, Switzerland. Corresponding author S. Gayadeen. Tel. +44(0)01235 778868. Fax +44(0)01235 778499.

Email addresses: sandira.gayadeen@diamond.ac.uk (Sandira Gayadeen), stephen.duncan@eng.ox.ac.uk (Stephen R. Duncan).

increase and thereby increasing the emittance of the photon beam. This in turn degrades the brilliance of the photon beam used in experiments and in turn, degrades the quality of the experiments carried out on the beamlines. In order to preserve the quality of the photon beam at Diamond, a controller is used to stabilise the electron beam by controlling the beam position to within 10% of the beam size, which corresponds to maintaining an RMS variation of less than 12.3μm in the horizontal plane and 0.6μm in the vertical plane [Rowland et al., 2007].

A feedback system is used to achieved the stability required of the electron beam which uses 172 electron beam position monitors (BPMs) to detect the electron beam position around the ring in both horizontal and vertical planes and varies the current to 172 small dipole magnets (referred to corrector magnets) in each plane to change the induced magnetic field in order to correct the position of the electron beam. The control update rate is 100μs, however the time taken to compute the control action is required to be less than 5μs where data acquisition and processing comprises the rest of the sample time. The high dimensional and multivariable nature of the control problem, coupled with the fast computation time requires that the structure of the problem is exploited to both reduce the multivariable nature and the computational burden. A key property of the process is that all the actuators have the same dynamics but have different steady state responses, so that the process is described by simple dynamics but a generally ill-conditioned steady state matrix. Following the approach of cross-directional control systems which generally exhibit these properties [Corscadden and Duncan, 2000, Duncan and Bryant, 1997, Featherstone et al., 2000, Heath, 1996], the steady state matrix is decomposed using orthogonal basis functions to identify and decouple the controllable modes of the system. This decomposition of the steady state response matrix allows controller dynamics for individual modes to be designed independently and simplifies tuning of the large-scale multivariable controller. For the Diamond Light Source system, an Internal Model Control (IMC) approach is used to select the controller dynamics for each mode because of the simplicity of tuning for performance and robustness since the process dynamics are inherently stable [Duncan, 2007, Gayadeen and Duncan, 2012, 2013, 2014],.

Synchrotron control systems usually include slew rate limits in the power supplies for the corrector magnets to impose current limitations to protect the corrector magnets. When these limits have been reached, the rate limiter acts as a restricted tracking problem and causes performance deterioration. In this paper, an anti-windup augmentation scheme is proposed to ensure that acceptable closed-loop performance is achieved when the corrector magnet power supplies are rate limited. The main goal is to provide some augmentation to the unconstrained IMC structure to provide anti-windup compensation for the rate limited systems. Moreover, because of the highly multivariable nature of the process, difficulties arise when tuning an anti-windup compensator, so the goal is to exploit the "modal" projection used to design the unconstrained IMC controller so that the anti-windup compensators can be tuned on a mode by mode basis as well. Another consideration to the performance of the anti-windup compensators is the effect of spatial uncertainties arising from beam optics [Gayadeen and Duncan, 2012], such that any augmentation to the unconstrained controller is required to preserve as much as possible the robustness of the unsaturated closed loop to such uncertainties.

The IMC structure has been shown to possess inherent anti-windup characteristics for saturating systems [Campo and Morari, 1990, Morales et al., 2013, Turner et al., 2003]. However the nonlinear performance may be sluggish and therefore enhancements to the IMC structure have been suggested to improve the nonlinear closed loop performance for saturating actuators by factorising the unconstrained IMC controller to include a forward controller and a feedback term around the saturation [Goodwin et al., 1993, Zheng et al., 1993]. IMC factorisations using a simple weighting on the forward and feedback term [Goodwin et al., 1993] and a more general approach [Zheng et al., 1993] were adapted for the electron beam stabilisation system under rate constraints [Gayadeen and Duncan, 2013]. However the techniques are restrictive in the parametrisation of the factorisation of the unconstrained IMC controller and the design was based on intuition. Furthermore, the factorisation choices showed that the achieved constrained performance was not acceptable for synchrotron electron beam positioning control [Gayadeen and Duncan, 2013, 2014]. The goal of the approach presented in this paper is to systematically parameterise the IMC anti-windup compensators on a mode by mode basis to ensure that some global performance target is met. However, the anti-windup technique developed in this paper takes a more general approach and is based on the framework introduced in Sofrony et al. [2010] for continuous time anti-windup synthesis for systems with rate limits using Riccati equations. In this paper, a discrete-time Riccati-based solution is proposed using a general anti-windup framework in which the anti-windup compensator is applied to the difference between the linear and nonlinear signal [Mulder et al., 2001, Turner et al., 2003, Weston and Postlethwaite, 2000]. The Riccati based solution is attractive instead of an LMI-based formulation because it is more straightforward to tune, with a single parameter that captures the trade-off between performance and robustness for rate constrained actuators. Moreover an LMI-based solution would be more computationally intensive for such systems with over 1000 states and sample rates greater than 10kHz.

For this application, the main purpose of anti-windup is to mitigate performance degradations by rate limiters. The linear controller is designed under nominal conditions and is augmented to provide anti-windup compensation. However, the robustness of the anti-windup system in the presence of plant uncertainty must be addressed. An Integral Quadratic Constraints (IQC) framework was used in Morales et al. [2013], where the robustness of the modified IMC structure for saturation constraints was compared to the standard framework in Weston and Postlethwaite [2000] and in this paper, an IQC framework is also used to develop conditions for robustness preservation of the modified IMC structure for rate constraints in the presence of norm-bounded uncertainty. However, extending an IQC approach to rate limiters is not straightforward since the discrete-time rate limiter structure is not stable in an l_2 sense and standard IQC based techniques rely on the interconnections of l_2 bounded systems. The approach taken in Gayadeen and Duncan [2013] is based on Megretski [2001] where the rate limiter is modified by including a first-order filter after the nonlinearity and a more detailed proof of the result given in Gayadeen and Duncan [2013] is presented in this paper. Furthermore, the robust stability test is used to determine how the allowable size of uncertainty is affected when the anti-windup augmentation of the constrained system is included.

The paper is organised as follows. In the following section, the process and rate limiter structure under consideration is described. In Section 3, the Riccati-based anti-windup design is developed and in Section 4, the IMC anti-windup structure for implementation is developed. In Section 5 the robust stability of the IMC anti-windup augmented closed loop in the presence of plant uncertainty is developed within an IQC framework. The IMC-based anti-windup compensators synthesized using a Riccati-based method was implemented on the booster synchrotron at Diamond Light Source. Machine data showing the performance of the implemented controller is presented and the robust stability of the structure is assessed in Section 6.

2 System under consideration

The open loop behaviour of the position of an electron beam in a synchrotron is well approximated by [Duncan, 2007, Gayadeen, 2014]

$$y[k] = g(z^{-1})Ru[k] + h[k] \tag{1}$$

where $u[k] \in \mathbb{R}^N$ are the inputs to the $N \in \mathbb{Z}^+$ corrector magnets, $h[k] \in \mathbb{R}^M$ is an external disturbance and $y[k] \in \mathbb{R}^M$ represents the deviation of the electron beam position from the ideal orbit in either horizontal or vertical directions measured at $M \in \mathbb{Z}^+$ sensors at times $\{t = kT_s : k \in \mathbb{Z}^+\}$, with T_s being the sample interval, so

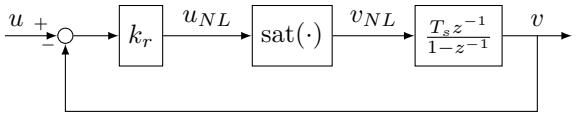

Fig. 1. Rate limiter structure

that $y[k] = y(kT_s)$. The dynamics are represented by the scalar $g(z^{-1})$ which is a first order response plus a delay [Duncan, 2007, Gayadeen, 2014]. The static response, $R \in \mathbb{R}^{M\times N}$, is a map from actuator to sensor position which captures the DC response of the actuators to a change in the transverse orbit position measured at mth sensor due to a transverse change in the magnetic field at the nth corrector magnet. For $M \leq N$, the response matrix can be expressed in terms of a reduced singular value decomposition such that,

$$R = \Phi[\Sigma \quad 0]\begin{bmatrix}\Psi_1^{\mathrm{T}} \\ \Psi_2^{\mathrm{T}}\end{bmatrix} \tag{2}$$

where $\Phi \in \mathbb{R}^{M\times M}$ are the left singular vectors, $\Psi_1 \in \mathbb{R}^{N\times M}$ and $\Psi_2 \in \mathbb{R}^{N\times(N-M)}$ are the right singular vectors, and $\Sigma \in \mathbb{R}^{M\times M}$ is a diagonal matrix containing the singular values, $\sigma_1 \geq \sigma_2 \geq \cdots \geq \sigma_M$. Therefore (1) can be written as

$$\Phi^{\mathrm{T}} y[k] = g(z^{-1})\Sigma\Psi_1^{\mathrm{T}} u[k] + \Phi^{\mathrm{T}} h[k] \tag{3}$$

Defining $\bar{y}[k] = \Phi^{\mathrm{T}} y[k]$, $\bar{u}[k] = \Psi_1^{\mathrm{T}} u[k]$ and $\bar{h}[k] = \Phi^{\mathrm{T}} h[k]$ projects the response into modal space, so that for each mode,

$$\bar{y}_m[k] = g(z^{-1})\sigma_m \bar{u}_m[k] + \bar{h}_m[k] \tag{4}$$

where $\bar{y}_m[k]$, $\bar{u}_m[k]$ and $\bar{h}_m[k]$ are the m^{th} elements of $\bar{y}[k]$, $\bar{u}[k]$ and $\bar{h}[k]$ so that each mode is controlled independently. Typically, the input signal applied to each actuator, $u_n[k]$ is rate constrained such that $-u_{rl}^{lim} \leq u_n[k] - u_n[k-1] \leq u_{rl}^{lim}$. For each input signal the rate limiter is modelled as a magnitude saturation cascaded with an integrator and a gain and enclosed in a feedback loop as depicted in Fig. 1, such that

$$v_n[k] = \frac{T_s z^{-1}}{1 - z^{-1}} \mathrm{sat}(k_r(u_n[k] - v_n[k])) \tag{5}$$

with $\mathrm{sat}(\cdot)$ being a saturation function defined by

$$\begin{aligned}\mathrm{sat}(u_{NL}[k]) &= \left[\mathrm{sat}(u_{NL_1}[k]) \ \ldots \ \mathrm{sat}(u_{NL_N}[k])\right]^{\mathrm{T}} \\ \mathrm{sat}(u_{NL_n}[k]) &= \min\{|u_{NL_n}[k]|, u_{sat}^{lim}\} \times \mathrm{sign}(u_{NL_n}[k])\end{aligned} \tag{6}$$

where u_{sat}^{lim} is the magnitude at which the input signal saturates and k_r is a gain. This representation is attractive for two reasons: firstly it represents the practical implementation of the rate limiter and secondly the nonlinear part of the actuator is simply the saturation

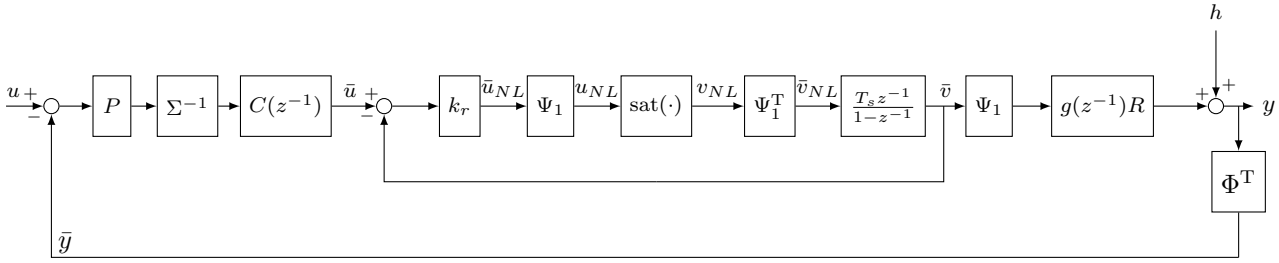

Fig. 2. Closed loop system with rate limiter.

function to which magnitude saturation anti-windup techniques can be applied. Assuming the presence of a controller that stabilises $g(z^{-1})R$, the system behaves linearly and the closed loop is asymptotically stable and well-posed when the saturation is not active. From (5), when the rate limits have not been reached (i.e. the saturation block acts as the identity), the rate limiter behaves as a low pass filter with cut-off frequency determined by k_r when $k_r T_s < 1$. At Diamond, $k_r = 1/T_s$ is chosen so that when the rate limits have been reached, the rate limiter is interpreted as a restricted tracking problem [Sofrony et al., 2010].

3 Riccati-based Anti-Windup Synthesis

For the nominal, unconstrained process the control signal is given by

$$u[k] = -\Psi_1 P \Sigma^{-1} C(z^{-1}) \Phi^{\mathrm{T}} y[k] \tag{7}$$

and in mode space this becomes

$$\bar{u}[k] = -P \Sigma^{-1} C(z^{-1}) \bar{y}[k] \tag{8}$$

where P and $C(z^{-1})$ are diagonal matrices with M elements. The gain matrix P is included because the response matrix, R is ill-conditioned so P is selected to limit control at the high order modes [Duncan, 2007, Gayadeen and Duncan, 2013, 2014]. When the rate limiter, $\varphi(\cdot)$ is active, the input to each actuator is constrained, so that $v_n[k] = \varphi(u_n[k])$, the rate constraints are introduced to the controller with the condition,

$$u_{rl}^{lim} \leq [\Psi \bar{u}[k]]_n - [\Psi \bar{u}[k-1]]_n \leq u_{rl}^{lim} \tag{9}$$

such that (5) becomes

$$\bar{v}_n[k] = \frac{T_s z^{-1}}{1 - z^{-1}} \Psi_1^{\mathrm{T}} \mathrm{sat}(\Psi_1 k_r (\bar{u}_n[k] - \bar{v}_n[k])) \tag{10}$$

where $\bar{v}[k] = \Psi_1^{\mathrm{T}} v[k]$. This structure is depicted in Fig. 2 where it can be seen that the saturation nonlinearity internal to the rate limiter is the only nonlinearity. The plant and the controller can be augmented to represent the problem as an equivalent magnitude limit problem [Sofrony et al., 2010] where a modified plant $\tilde{G}(z^{-1})$ and a modified unconstrained controller $\tilde{C}(z^{-1})$ are defined as

$$\begin{aligned} \begin{bmatrix} \bar{y}[k] \\ \bar{v}[k] \end{bmatrix} &= \underbrace{\begin{bmatrix} g(z^{-1}) \frac{T_s z^{-1}}{1 - z^{-1}} \Sigma \\ \frac{T_s z^{-1}}{1 - z^{-1}} I \end{bmatrix}}_{\tilde{G}(z^{-1})} \bar{v}_{NL}[k] + \begin{bmatrix} I \\ 0 \end{bmatrix} \bar{h}[k] \\ \bar{u}_{NL}[k] &= \underbrace{k_r \begin{bmatrix} -P \Sigma^{-1} C(z^{-1}) & -I \end{bmatrix}}_{\tilde{C}(z^{-1})} \begin{bmatrix} \bar{y}[k] \\ \bar{v}[k] \end{bmatrix} \end{aligned} \tag{11}$$

with $\bar{v}_{NL}[k] = \Psi_1^{\mathrm{T}} v_{NL}[k]$ and $\bar{u}_{NL}[k] = \Psi_1^{\mathrm{T}} u_{NL}[k]$. The rate limit problem can now be considered as a standard magnitude saturation problem with a plant $\tilde{G}(z^{-1})$ driven by the signal $\bar{v}_{NL}[k]$ and a controller $\tilde{C}(z^{-1})$ producing the control signal $\bar{u}_{NL}[k]$.

The anti-windup compensator, $X(z^{-1})$ is driven by $\tilde{v}_{NL} := \bar{u}_{NL} - \bar{v}_{NL} = \mathrm{Dz}(\bar{u}_{NL})$ where $\mathrm{Dz}(\cdot)$ represents the deadzone nonlinearity and the outputs, v_d and y_d of the anti-windup compensator are injected into the controller's input and output respectively [Sofrony et al., 2010]. This anti-windup structure takes the form shown in Fig. 3 [Weston and Postlethwaite, 2000] where the closed loop equations for this structure are given as,

$$\begin{aligned} u_{NL}[k] &= \Psi_1 \left(u_{lin}[k] - v_d[k] \right) \\ v_d[k] &= \left(X(z^{-1}) - I \right) \Psi_1^{\mathrm{T}} \left(u_{NL}[k] - v_{NL}[k] \right) \\ u_{lin}[k] &= k_r \left(\bar{u}[k] - v_{lin}[k] \right) \\ \bar{u}[k] &= P \Sigma^{-1} C(z^{-1}) \left(y_d[k] + \bar{y}[k] \right) \\ v_{lin}[k] &= \bar{v}[k] + v_{rd}[k] \\ y_d[k] &= g(z^{-1}) \frac{T_s z^{-1}}{1 - z^{-1}} \Sigma X(z^{-1}) \Psi_1^{\mathrm{T}} \left(u_{NL}[k] - v_{NL}[k] \right) \\ \bar{v}[k] &= \frac{T_s z^{-1}}{1 - z^{-1}} \Psi_1^{\mathrm{T}} v_{NL}[k] \\ v_{rd}[k] &= \frac{T_s z^{-1}}{1 - z^{-1}} X(z^{-1}) \Psi_1^{\mathrm{T}} \left(u_{NL}[k] - v_{NL}[k] \right) \end{aligned} \tag{12}$$

The state space realisation of the modified plant has a larger state vector as it includes dynamics absorbed from

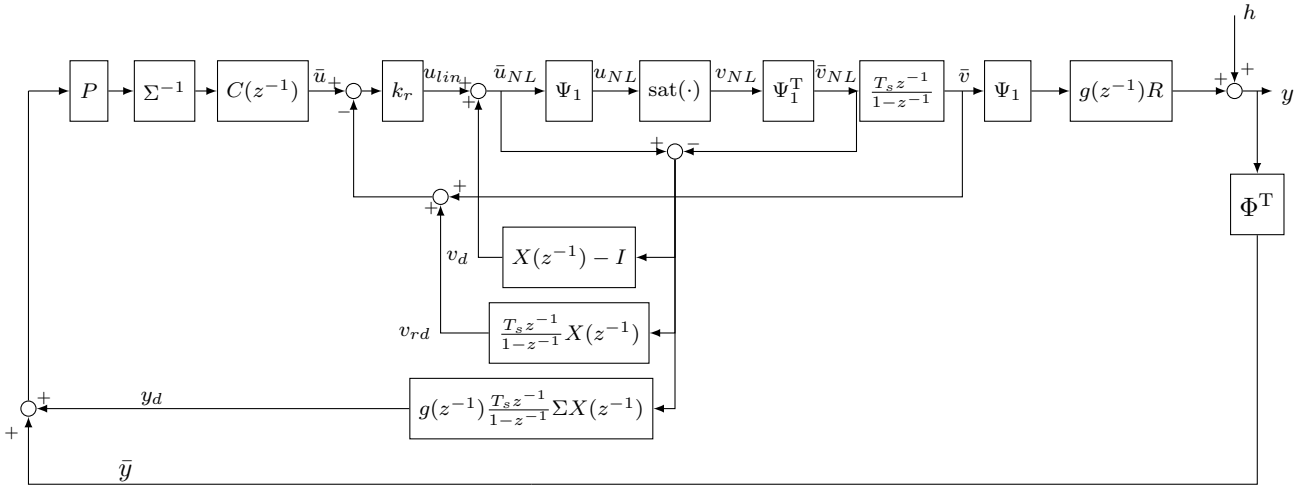

Fig. 3. Closed loop anti-windup system for Riccati-based formulation

the rate limiter and is given as

$$\tilde{G}(z^{-1}) \sim \left[\begin{array}{c|c} \mathcal{A}_{\tilde{G}} & \mathcal{B}_{\tilde{G}} \\ \hline \mathcal{C}_{\tilde{G}} & \mathcal{D}_{\tilde{G}} \end{array}\right] \tag{13}$$

Since the integrator in Fig. 1 is strictly proper, $\mathcal{D}_{\tilde{G}} = 0$ for the system under consideration. The anti-windup compensator, which is based on the right co-prime factorisation of the plant, has the structure

$$\begin{bmatrix} X(z^{-1}) - 1 \\ \tilde{G}(z^{-1}) X(z^{-1}) \end{bmatrix} \sim \left[\begin{array}{c|c} \mathcal{A}_{\tilde{G}} + \mathcal{B}_{\tilde{G}} \mathcal{F}_{\tilde{G}} & \mathcal{B}_{\tilde{G}} \\ \hline \mathcal{F}_{\tilde{G}} & 0 \\ \mathcal{C}_{\tilde{G}} & 0 \end{array}\right] \tag{14}$$

which is parameterised by the free parameter $\mathcal{F}_{\tilde{G}}$ such that $\mathcal{A}_{\tilde{G}} + \mathcal{B}_{\tilde{G}} \mathcal{F}_{\tilde{G}}$ is Hurwitz [Sofrony et al., 2010]. The anti-windup problem can be defined by the map from the linear control signal u_{lin} to the perturbation to the output $\tilde{y}_d := \left[\bar{y}[k]^{\mathrm{T}} \; \bar{v}[k]^{\mathrm{T}}\right]^{\mathrm{T}}$ i.e. $\mathcal{T} : u_{lin} \mapsto y_d$. Therefore the gain of $\mathcal{T}$ dictates how much the linear performance degrades in the presence of the rate constraint. The state space realisation of $\mathcal{T}$ is given by

$$\mathcal{T} \sim \begin{cases} \tilde{x}[k+1] = \left(\mathcal{A}_{\tilde{G}} + \mathcal{B}_{\tilde{G}} \mathcal{F}_{\tilde{G}}\right) \tilde{x}[k] + \mathcal{B}_{\tilde{G}} \tilde{v}_{NL}[k] \\ v_d[k] = \mathcal{F}_{\tilde{G}} \tilde{x}[k] \\ \tilde{y}_d[k] = \mathcal{C}_{\tilde{G}} \tilde{x}[k] \\ \tilde{v}_{NL} = \varphi\left(u_{lin}[k] - v_d[k]\right) \end{cases} \tag{15}$$

for any Lipschitz nonlinear element $\varphi(\cdot) \in \text{Sector}[0, \epsilon I]$. The performance of the anti-windup compensator can be measured using the l_2 gain, $\|\mathcal{T}\|_2$. The goal is to find a feedback gain $\mathcal{F}_{\tilde{G}}$ (and hence $X(z^{-1})$) such that the upper bound of the l_2 gain of $\mathcal{T}$ is minimised, i.e. $\|\mathcal{T}\|_2 \leq \gamma$ for sufficiently small γ. A systematic way of computing $\mathcal{F}_{\tilde{G}}$ based on a Riccati approach is presented in the following Theorem.

Theorem 1 *There exists a full order anti-windup compensator guaranteeing global asymptotic stability of the origin of $\mathcal{T}$ and ensuring $\|\mathcal{T}\|_2 \leq \gamma$ as stated in* (14)*, if there exists matrix $\mathcal{P} = \mathcal{P}^{\mathrm{T}} > 0$, diagonal matrix $\mathcal{W} > 0$ and positive real scalars γ and $\epsilon \in (0, 1)$ such that the following Riccati equation is satisfied*

$$\begin{aligned} &\mathcal{A}_{\tilde{G}}{}^{\mathrm{T}} \mathcal{P} \mathcal{A}_{\tilde{G}} - \mathcal{P} + \mathcal{C}_{\tilde{G}}{}^{\mathrm{T}} \mathcal{C}_{\tilde{G}} - \mathcal{A}_{\tilde{G}}{}^{\mathrm{T}} \mathcal{P} \mathcal{B}_{\tilde{G}} \\ &\left(\epsilon^{-2} \mathcal{W}^{-2} Z - 2\epsilon^{-1} \mathcal{W}^{-1} - I\right) \mathcal{B}_{\tilde{G}}{}^{\mathrm{T}} \mathcal{P} \mathcal{A}_{\tilde{G}} = 0 \end{aligned} \tag{16}$$

where $Z = 2\mathcal{W} - \mathcal{B}_{\tilde{G}}^{\mathrm{T}} \mathcal{P} \mathcal{B}_{\tilde{G}} - \gamma^{-2} \epsilon^2 \mathcal{W}^2$ and a suitable anti-windup compensator described by (14) *is obtained from*

$$\begin{aligned} \mathcal{F}_{\tilde{G}} = &- \left(\frac{(2-\epsilon)}{\epsilon^2} \mathcal{W}^{-1} - \frac{1}{\gamma^2} I - \frac{1}{\epsilon^2} \mathcal{W}^{-2} \mathcal{B}_{\tilde{G}}^{\mathrm{T}} \mathcal{P} \mathcal{B}_{\tilde{G}}\right) \\ &\mathcal{B}_{\tilde{G}}{}^{\mathrm{T}} \mathcal{P} \mathcal{A}_{\tilde{G}} \end{aligned} \tag{17}$$

Proof See Appendix A.

For a given γ, and therefore for a given performance bound, there exists a family of compensator gains $\mathcal{F}_{\tilde{G}}$ parameterised by $\epsilon \in (0, 1)$. Note that the nonlinearity can be described to inhabit a narrower sector when $\epsilon \neq 1$ thereby restricting the set of possible signals u_{NL}, so that the results are local rather than global. From (17), when ϵ approaches 0, the norm of $\mathcal{F}_{\tilde{G}}$ increases, so that from (14), γ is as small as possible and the best performance is achieved. Conversely, when ϵ tends to unity, $\mathcal{F}_{\tilde{G}}$ becomes small and γ is large, which corresponds to the worst performance.

4 IMC-based Anti-Windup Structure

The controller architecture in Fig. 3 is difficult to realise for physical rate limits since, in most cases, the

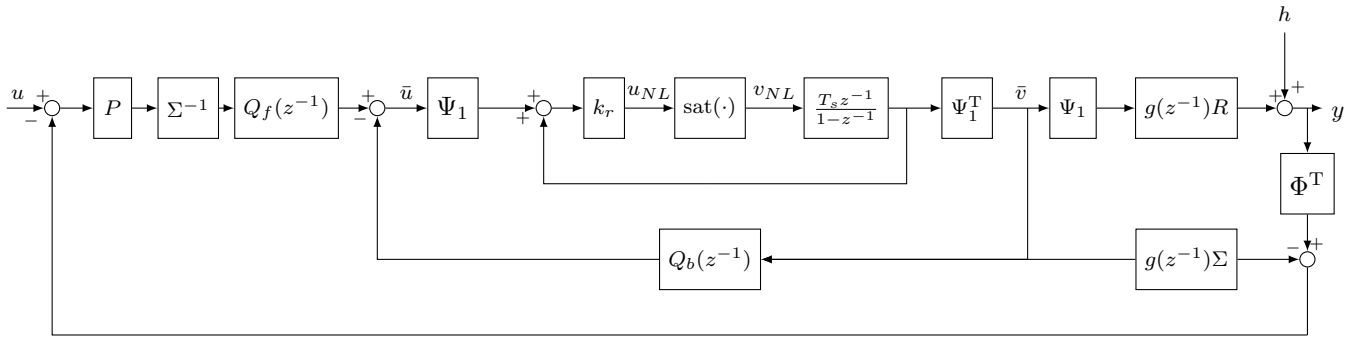

Fig. 4. Closed loop IMC structure with rate limiter in modal form

saturation block cannot be directly accessed. Instead an IMC structure offers a natural framework for anti-windup compensation where a parallel path containing a model of the nominal process is included such that the control signal is given by

$$\begin{aligned}\bar{u}[k] &= -P\Sigma^{-1}Q(z^{-1})\bar{h}[k] \\ \bar{y}[k] &= \bar{h}[k] + g(z^{-1})\Sigma\bar{u}[k]\end{aligned} \tag{18}$$

where the diagonal matrix P is as before and $Q(z^{-1}) = \text{diag}_{m=1,\ldots,M}\{(q_m(z^{-1})\}$ is the IMC filter, so that the controller dynamics for each mode are given by

$$C(z^{-1}) = \Psi\text{diag}\left(\frac{\sigma_m^{-1}p_m q_m(z^{-1})}{1 - p_m q_m(z^{-1})g(z^{-1})}\right)\Phi^{\mathrm{T}} \tag{19}$$

When the input to each actuator is constrained, a model of the rate limiter must also be included in the parallel path with the process model so that the nominal closed loop equations become

$$\begin{aligned}\bar{u}[k] &= -P\Sigma^{-1}Q(z^{-1})\bar{h}[k] \\ \bar{y}[k] &= \bar{h}[k] + g(z^{-1})\Sigma\bar{v}[k]\end{aligned} \tag{20}$$

Improved dynamic response under constraints is gained by including a feedback term around the non-linearity when the non-linear element is a saturation [Zheng et al., 1993] by factorising the unconstrained controller, $Q(z^{-1})$ into $Q_f(z^{-1}) = \text{diag}_{m=1,\ldots,M}\{q_f(z^{-1})\}$ and $Q_b(z^{-1}) = \text{diag}_{m=1,\ldots,M}\{q_b(z^{-1})\}$. On a mode-by-mode basis, the factorisation is described by

$$q_m(z^{-1}) = \frac{q_{f_m}(z^{-1})}{1 + q_{b_m}(z^{-1})} \tag{21}$$

where $q_{b_m}(z^{-1})$ is in the feedback loop around the saturation nonlinearity. However, for the rate limiter structure shown in Fig. 1, the factorisation becomes

$$q_m(z^{-1}) = q_{f_m}(z^{-1})\frac{k_r T_s z^{-1}}{1 - \left[1 - k_r T_s - k_r T_s q_{b_m}(z^{-1})\right] z^{-1}} \tag{22}$$

such that when the system is unconstrained, $q_{f_m}(z^{-1})$ and $q_{b_m}(z^{-1})$ are equivalent to the unconstrained controller and the anti-windup augmentation does not affect the closed loop behaviour.

The IMC anti-windup structure for a rate limit nonlinearity takes the form shown in Fig. 4 for the system under consideration and the control action is given by

$$\begin{aligned}&\bar{u}[k] = -P\Sigma^{-1}Q_f(z^{-1})\bar{y}[k] + \\ &\left[Pg(z^{-1})Q_f(z^{-1}) - Q_b(z^{-1})\right]\bar{v}[k] \\ &\bar{v}[k] = \Psi_1^{\mathrm{T}}\frac{T_s z^{-1}}{1 - z^{-1}}v_{NL}[k] \\ &u_{NL}[k] = -k_r\Psi_1 P\Sigma^{-1}Q_f(z^{-1})\bar{y}[k] + K_r\Psi_1 \\ &\left[Pg(z^{-1})Q_f(z^{-1}) - Q_b(z^{-1}) - I\right]\Psi_1^{\mathrm{T}}\frac{T_s z^{-1}}{1 - z^{-1}}v_{NL}[k]\end{aligned} \tag{23}$$

The structure in Fig. 3 is equivalent to the IMC structure in Fig. 4 for some choice of $X(z^{-1})$, $Q_f(z^{-1})$ and $Q_b(z^{-1})$, so the compensator designed using Theorem 1 can be used to synthesise IMC anti-windup compensators $Q_f(z^{-1})$ and $Q_b(z^{-1})$. By comparing (12) and (23), Fig. 4 is equivalent to the structure in Fig. 3 if $X(z^{-1})$) is invertible and

$$\begin{aligned}Q_f(z^{-1}) &= -\left[X(z^{-1})\right]^{-1}\left[A(z^{-1})\right]^{-1}C(z^{-1}) \\ Q_b(z^{-1}) &= \frac{1}{\bar{\varphi}(z^{-1})}\left[\left[X(z^{-1})\right]^{-1} - I\right] - I\end{aligned} \tag{24}$$

where

$$\begin{aligned}A(z^{-1}) &= I + \bar{\varphi}(z^{-1})\left[I - g(z^{-1})PC(z^{-1})\right] \\ \bar{\varphi}(z^{-1}) &= \frac{k_r T_s z^{-1}}{1 - z^{-1}}\end{aligned} \tag{25}$$

Furthermore, if $X(z^{-1})$ is chosen as

$$X(z^{-1}) = \frac{1 - z^{-1}}{1 - (1 - k_r T_s)z^{-1}}I \tag{26}$$

the standard IMC structure (with no anti-windup compensation) is recovered, i.e. $Q_b(z^{-1}) = 0$ and

$$Q_f(z^{-1}) = \frac{1-(1-k_rT_s)z^{-1}}{k_rT_sz^{-1}}Q(z^{-1}) \tag{27}$$

The Riccati-based synthesis of $Q_f(z^{-1})$ and $Q_b(z^{-1})$ can be used to parameterise other commonly used IMC factorisations, such as

$$Q_f(z^{-1}) = \beta(z^{-1})g^-(z^{-1})Q(z^{-1}) \tag{28}$$

where $g^-(z^{-1})$ represents the minimum phase components of $g(z^{-1})$ and $\beta(z^{-1})$ is a filter which is usually designed based on intuition [Zheng et al., 1993]. The formulation in (28) can be interpreted in terms of the parameterisation given by $X(z^{-1})$ where

$$\beta(z^{-1}) = \left[g^-(z^{-1})\bar{\varphi}(z^{-1})X_r(z^{-1})\right]^{-1} \tag{29}$$

so that an appropriate $\beta(z^{-1})$ is directly determined based on a performance operator $\mathcal{T}$.

5 Robust Stability of Anti-Windup Augmented Closed Loop

For the design of the unconstrained controller and the anti-windup augmentation, the nominal system was considered and the anti-windup system has a performance index given by γ. In this section, a norm-bounded uncertainty associated with the spatial response of the system is included and the robust stability of the IMC anti-windup augmented closed loop is determined. The robust stability of the anti-windup augmented closed loop can be addressed via the minimisation of the l_2 gain, but due to the presence of the integrator term in the rate limiter model, the interconnection of the rate limiter is not l_2 stable, a condition required for analysis within the IQC framework. The l_2 stability problem is resolved by connecting the rate limiter in series with a filter [Megretski, 2001] so that $w_n[k] = \rho(z^{-1})v_n[k]$, and a modified rate limiter is defined as

$$\tilde{\varphi}(z^{-1}) = \varphi(\cdot)\rho(z^{-1}) \tag{30}$$

For this application $k_r = 1/T_s$, so that when the saturation acts as the identity, $\tilde{\varphi}(z^{-1}) = z^{-1}\rho(z^{-1})$ and an appropriate choice for the filter is $\rho(z^{-1}) = 1/z^{-1}$. The l_2 stability of the modified rate limiter with this choice can be determined as described in the following Lemma.

Lemma 1 (l_2 stability of discrete rate limiter) *For the semiconcave function* sat *with* $\frac{\partial \mathrm{sat}(u)}{\partial u}|_{u=0} = \kappa$ *for* $0 < \kappa < \infty$, *define* $\tilde{\varphi}$ *as the system* $u_n[k] \to w_n[k]$ *where*

$$\begin{aligned} v_{NL}[k] &= \mathrm{sat}(k_r(u_n[k] - v_n[k])) \\ w_n[k] &= v_n[k] + T_s\mathrm{sat}(k_r(u_n[k] - v_n[k])) \end{aligned} \tag{31}$$

and $v_n(0) = 0$, *the system is stable and the induced* l_2 *gain in the channel* $u_n[k] \to w_n[k]$ *does not exceed* $\max\{\kappa, \sqrt{2}\}$.

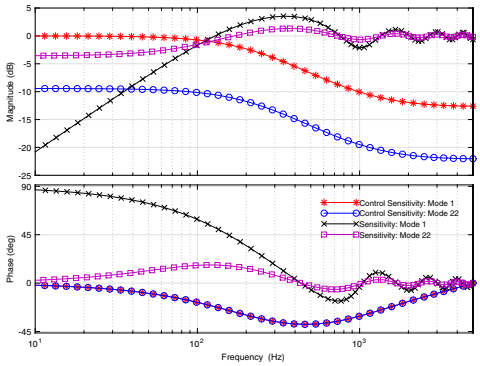

Fig. 5. Control sensitivities for mode 1 ('$*$' red) and mode 22 ('o' blue) and closed loop sensitivity for mode 1 ('x' black) and mode 22 ('□' magenta) for the nominal system.

Proof See Appendix B.

Because the modified rate limiter was used in (30), the plant model is adjusted to reflect the modified rate limiter in order to preserve the original problem by introducing a filter $1/\rho(z^{-1})$ at the input to the plant, such that $g_{rl}(z^{-1}) = z^{-1}g(z^{-1})$. Although for the choice $\rho(z^{-1}) = 1/z^{-1}$, only the non-minimum phase characteristics of the plant is modified. The control law for the modified rate limiter and plant within the IMC structure in Fig. 4 becomes,

$$\begin{aligned} \bar{u}[k] &= -P\Sigma^{-1}Q_f(z^{-1})\left(\bar{y}[k] - g_{rl}(z^{-1})\Sigma\bar{w}[k]\right) \\ \bar{w}[k] &= \Psi_1^{\mathrm{T}}\rho(z^{-1})v[k] \\ v[k] &= \frac{T_sz^{-1}}{1-z^{-1}}\mathrm{sat}\left(k_r(u[k] - v[k])\right) \end{aligned} \tag{32}$$

However, given the choices of $g_{rl}(z^{-1})$ and $\rho(z^{-1})$, $\bar{u}[k]$ for the modified system is equivalent to the original problem, so that $Q(z^{-1})$ designed for the modified rate limiter and the plant, provides the desired input for the original problem.

5.1 Robust Stability Analysis with IQCs

To guarantee external stability of the closed loop when the IMC anti-windup system is augmented to include spatial uncertainty, both the uncertainty and the

nonlinearity can be expressed in an IQC framework. For the following perturbed system,

$$y[k] = \Phi g(z^{-1}) \left[\Sigma + \Delta_\Sigma\right] \Psi_1^{\mathrm{T}} u[k] + h[k] \tag{33}$$

the operator Δ_Σ is considered to be diagonal to represent independent variations in each mode. For stability analysis, it is advantageous to represent the closed loop system in the standard feedback loop configuration [Megretski and Rantzer, 1997], where the operator Δ_Σ is defined by $v_\Delta[k] = \Delta_\Sigma u_\Delta[k]$ and $w[k] = \tilde{\varphi} u[k]$, so that the closed loop system is completely characterized by

$$\begin{aligned} \begin{bmatrix} u[k] \\ u_{\Delta_\Sigma}[k] \end{bmatrix} &= \mathcal{M}(z^{-1}) \begin{bmatrix} w[k] \\ v_{\Delta_\Sigma}[k] \end{bmatrix} \\ \begin{bmatrix} w[k] \\ v_{\Delta_\Sigma}[k] \end{bmatrix} &= \Delta_T \left(\begin{bmatrix} u[k] \\ u_{\Delta_\Sigma}[k] \end{bmatrix} \right) \end{aligned} \tag{34}$$

where the operator Δ_T encapsulates the rate limiter and the uncertainty such that, $\Delta_T = \mathrm{diag}\{\tilde{\varphi}, \Delta_\Sigma\}$ and the linear time invariant transfer matrix $\mathcal{M}(z^{-1})$ is given as,

$$\begin{bmatrix} -\Psi_1 Q_b(z^{-1}) \Psi_1^{\mathrm{T}} & -\Psi_1 P \Sigma^{-1} g_{rl}(z^{-1}) Q_f(z^{-1}) \\ \Psi_1^{\mathrm{T}} & 0 \end{bmatrix} \tag{35}$$

For mixed uncertainty, $\Delta_\Sigma \in \mathrm{IQC}(\Pi_{\Delta_\Sigma})$ and $\tilde{\varphi} \in \mathrm{IQC}(\Pi_{\tilde{\varphi}})$ and in this case, the uncertainty is represented as $\Delta_\Sigma = \mathrm{diag}\{\delta_{\Sigma m}\}$ with $\|\delta_{\Sigma m}\|_\infty \leq 1$, $\forall m = 1 \ldots M$, so that

$$\Pi_{\Delta_\Sigma} = \begin{bmatrix} \Gamma_{\Delta_\Sigma} & 0 \\ 0 & -\Gamma_{\Delta_\Sigma} \end{bmatrix} \tag{36}$$

is a suitable choice, where $\Gamma_{\Delta_\Sigma} = \mathrm{diag}\{\gamma_{\Delta_{\Sigma m}}\}$ and $\gamma_{\Delta_\Sigma} > 0$. From Lemma 1, an IQC multiplier can be derived from the relationship between the gain from $u_n[k]$ to $w_n[k]$, which is shown to not exceed $\sqrt{2}$, giving $\Pi_{\tilde{\varphi}_1} = [2I\ 0; 0\ -I]$. An IQC multiplier can also be derived from the relationship between the input and output of saturation block which can be modeled as a [0,1] sector bounded nonlinearity: $\Pi_{\tilde{\varphi}_2} = [0\ I; I\ -2I]$. Any conic combination of multipliers $\Pi_{\tilde{\varphi}_1}$ and $\Pi_{\tilde{\varphi}_2}$ are also considered as appropriate, so that $\Pi_{\tilde{\varphi}} = \sum_{i=1}^{2} k_\Pi \Pi_{\tilde{\varphi}_i}$ for any $k_\Pi \geq 0$ [Chakraborty et al., 2011].

If $\mathcal{M}(z^{-1})$ has the state space representation, $\mathcal{M}(z^{-1}) = \mathcal{C}_\mathcal{M}(z^{-1}I - \mathcal{A}_\mathcal{M})^{-1}\mathcal{B}_\mathcal{M} + \mathcal{D}_\mathcal{M}$ such that the pair $(\mathcal{A}_\mathcal{M}, \mathcal{B}_\mathcal{M})$ is controllable and $\mathcal{A}_\mathcal{M}$ has no eigenvalues on the imaginary axis, then the frequency domain characterization of the main IQC condition from [Megretski and Rantzer, 1997] is that

$$\begin{bmatrix} \left(e^{j\omega} I - \mathcal{A}_\mathcal{M}\right) \mathcal{B}_\mathcal{M} \\ I \end{bmatrix}^* \Pi \begin{bmatrix} \left(e^{j\omega} I - \mathcal{A}_\mathcal{M}\right) \mathcal{B}_\mathcal{M} \\ I \end{bmatrix} \leq -\theta I. \tag{37}$$

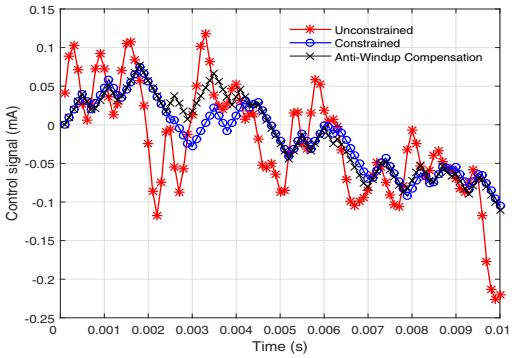

Fig. 6. Control signal to actuator when unconstrained ('∗' red), when constrained ('o' blue) and when constrained with anti-windup compensation ('x' black) of rate limiter over 0.01s period.

for some $\theta > 0$, where Π is structured as $\Pi = [\Pi_{11}\ \ \Pi_{12}; \Pi_{21}\ \ \Pi_{22}]$ [Morales and Heath, 2011] with

$$\begin{aligned} \Pi_{11} &= \mathcal{C}_\mathcal{M}^{\mathrm{T}} \Pi_{\Delta_T(11)} \mathcal{C}_\mathcal{M} \\ \Pi_{12} &= \Pi_{21}^* = \mathcal{C}_\mathcal{M}^{\mathrm{T}} \Pi_{\Delta_T(12)} + \mathcal{C}_\mathcal{M}^{\mathrm{T}} \Pi_{\Delta_T(11)} \mathcal{D}_\mathcal{M} \\ \Pi_{22} &= \Pi_{\Delta_T(22)} + \Pi_{\Delta_T(21)} \mathcal{D}_\mathcal{M} + \mathcal{D}_\mathcal{M}^{\mathrm{T}} \Pi_{\Delta_T(12)} + \\ &\quad \mathcal{D}_\mathcal{M}^{\mathrm{T}} \Pi_{\Delta_T(11)} \mathcal{D}_\mathcal{M} \end{aligned} \tag{38}$$

and $\Delta_T \in \mathrm{IQC}(\Pi_{\Delta_T})$ so that the uncertainty and rate limiter can be modeled with a convex combination of multipliers [Jonsson, 2001], such that $\Pi_{\Delta_T} = \mathrm{daug}\{\Pi_{\tilde{\varphi}}, \Pi_{\Delta_\Sigma}\}$ where $\mathrm{daug}(\cdot)$ represents a diagonal augmentation of the submultipliers [El Ghaoui and Niculescu, 2000]. By the discrete KYP Lemma [Rantzer, 1996], (37) is equivalent to satisfying the feasibility problem,

$$\Pi + \begin{bmatrix} \mathcal{A}_\mathcal{M}^{\mathrm{T}} \mathcal{G} \mathcal{A}_\mathcal{M} - \mathcal{G} & \mathcal{A}_\mathcal{M}^{\mathrm{T}} \mathcal{G} \mathcal{B}_\mathcal{M} \\ \mathcal{B}_\mathcal{M}^{\mathrm{T}} \mathcal{G} \mathcal{A}_\mathcal{M} & \mathcal{B}_\mathcal{M}^{\mathrm{T}} \mathcal{G} \mathcal{B}_\mathcal{M} \end{bmatrix} \leq 0 \tag{39}$$

such that there exists some matrix $\mathcal{G}^{\mathrm{T}} = \mathcal{G}$. Because Δ_Σ and Γ_{Δ_Σ} are diagonal, the stability condition can be decomposed on a mode by mode basis, so that there is a different $\gamma_{\Delta_{\Sigma m}}$ for each mode [Morales and Heath, 2011].

6 Booster Anti-Windup Design and Implementation

In the Diamond booster synchrotron, the same power electronics and corrector magnets are installed around the ring, so that all the same open loop dynamics, $g(z^{-1})$ are observed for each actuator-sensor pairing. However the steady state response is different, therefore $g(z^{-1})$ is represented as a scalar and the steady state responses are described by the response matrix, R. The dynamics are measured as a first order response, which is dominated by the power supplies for the corrector magnets and

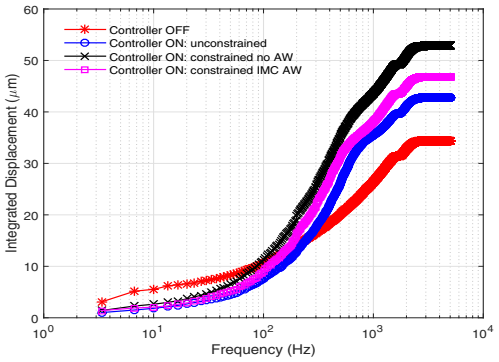

Fig. 7. Uncontrolled integrated beam motion at first vertical BPM on the booster ('∗' red) and controlled integrated beam motion for the unconstrained system ('o' blue), the rate constrained system with no anti-windup ('x' black) and rate constrained system with IMC anti-windup ('□' magenta) and for a rate limit of 1.5A/s.

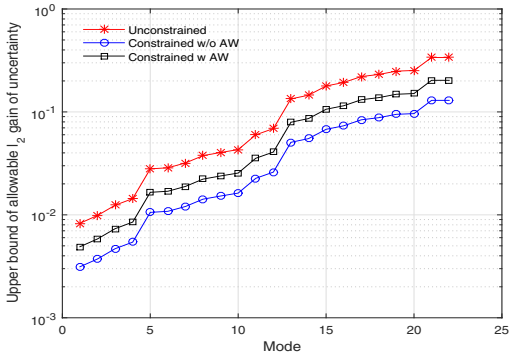

Fig. 8. Upper bound of allowable l_2 gain of δ_{Σ_m} on the booster for the unconstrained system ('∗' red), the rate constrained system without anti-windup ('o' blue) and with anti-windup compensation ('x' black). In all cases, $\mu = 1$.

a delay, arising from the sensor data acquisition and processing. The bandwidth of the booster actuator response was measured on the machine [Gayadeen, 2014, Gayadeen et al., 2011] and is given by

$$g(z^{-1}) = z^{-7}\frac{0.467z^{-1}}{1-0.534z^{-1}} \tag{40}$$

The IMC filter, $q_m(z^{-1})$, designed on a mode-by-mode basis is chosen by augmenting the approximate inverse of the plant dynamics with a first-order filter where the approximate inverse is given by inverting the minimum-phase component of the process such that

$$q_m(z^{-1}) = \frac{1-\lambda_m}{1-\lambda_m z^{-1}}\frac{1-0.534z^{-1}}{0.467z^{-1}} \tag{41}$$

where λ_m is the dominant closed-loop time constant when large enough and is chosen as $\lambda_m = e^{-\zeta_m T_s}$ where ζ_m is a tuning parameter which can be different for each mode [Gayadeen and Duncan, 2014, Morari and Zafiriou, 1989]. The controller gain is given by

$$\frac{p_m}{\sigma_m} = \frac{\sigma_m}{\sigma_m^2+\mu} \tag{42}$$

where the regularisation parameter, μ is chosen such that ${\sigma_m}^{-1}p_m \approx {\sigma_m}^{-1}$ when $\sigma_m^2 \gg \mu$ and ${\sigma_m}^{-1}p_m$ becomes small when $\sigma_m^2 \ll \mu$ [Gayadeen and Duncan, 2014]. The linear controller performance is demonstrated in Fig. 5, where the gain of the control sensitivity for the lower order modes is larger than the higher order modes to limit control at the higher order modes which correspond to small singular values. Furthermore, the bulk of the disturbance content lies in the low order modes and at frequencies below 100Hz [Gayadeen, 2014] so that the sensitivity for low order modes is chosen to be more aggressive at low frequencies than the higher order modes. However this is at the cost of amplifying disturbances at high frequencies although motion above 100Hz is not detected at the photon beam experimental stage, so the amplification is acceptable. When rate limits on the actuators are introduced, the main goal is to synthesize an anti-windup compensator which guarantees stability while preserving performance as much as possible. Theorem 1 is used to determine $\mathcal{F}_{\tilde{G}}$ with $\epsilon = 0.9$ (to demonstrate the anti-windup compensation performance) and because the IMC structure is more suitable for implementation, equivalent $Q_f(z^{-1})$ and $Q_b(z^{-1})$ were synthesized. Fig. 6 shows the control signal to the actuator for the linear case and when the rate limits are applied (with and without anti-windup compensation). When the rate limits are active, both the uncompensated and compensated systems suffer a lack of tracking ability, however it is difficult to conclude whether the tracking properties are improved with anti-windup. Instead the integrated beam motion (i.e. the integrated frequency response over frequency) observed on the booster at a single BPM is shown in Fig. 7 for the uncorrected beam position and the corrected beam position with and without constraints. The beam motion up to around 200Hz is suppressed for the linear controller and when the rate constraints are active, deterioration in performance is observed across all frequencies where the bandwidth is reduced to $<$ 100Hz. Moreover at higher frequencies the effect of the rate limiter is greatest as the tracking problem becomes more difficult. The IMC anti-windup compensation seeks to return the system to linear behaviour across all frequencies and the achieved bandwidth is 150Hz.

With $\epsilon = 0.9$, the robust stability test is used to determine an upper bound on the l_2 gain of the allowable spatial uncertainty for the constrained closed loop with and without anti-windup compensation. Fig. 8 shows the result for each mode where for the linear, constrained system, the upper bound on $\|\delta_{\Sigma_1}\|_\infty = 0.008$. When the

rate limits are introduced the size of allowable spatial uncertainty is reduced so that $\|\delta_{\Sigma_1}\|_\infty = 0.003$. However the inclusion of anti-windup compensation makes the mode more robust so that $\|\delta_{\Sigma_1}\|_\infty = 0.005$. The results are conservative since only uncertainty in the singular values are considered but the analysis can be extended to include other sources of spatial uncertainty appearing in Φ and Ψ [Gayadeen, 2014].

7 Conclusion

This paper has considered anti-windup synthesis based on IMC for rate constrained actuators for electron beam stabilisation control systems of synchrotrons. The common practice of factorising the unconstrained IMC controller to include a feedback term around a nonlinearity to improve constrained performance is applied to a rate limiter and a Riccati-based synthesis that guarantees constrained closed loop specifications is reformulated for the IMC anti-windup structure. The preservation of the IMC structure allows for minor modifications to be made to the unconstrained system in order to provide acceptable constrained performance when the actuator rate limits are active. Furthermore, the IMC anti-windup approach does not require signals from within the rate limiter structure to be accessed which is of practical importance for this application. An IQC robust stability test is developed to incorporate both the rate constraint and spatial uncertainty to ensure that the augmented closed loop system is robustly stable. The IMC anti-windup augmentation was implemented at the Diamond Light Source facility and resulted in acceptable performance while rate constrained.

Acknowledgements

The authors would like to thank Diamond Light Source Ltd. for supporting this research and for contributing to the experimental work carried out on the synchrotron. The authors would also like to acknowledge the Institute of Engineering and Technology (IET) for financial support through the IET Postgraduate Scholarship for an Outstanding Researcher awarded to S. Gayadeen. The authors also wish to thank the anonymous reviewers for their careful review and insightful comments and suggestions.

A Proof of Theorem 1

Proof The Lyapunov function candidate is chosen as $\mathcal{V} = \tilde{x}^{\mathrm{T}}\mathcal{P}\tilde{x} > 0$ (where $\tilde{x}$ is the shorthand notation for $\tilde{x}[k]$) and the Lyapunov difference defined as $\Delta\mathcal{V} := \mathcal{V}^+ - \mathcal{V}$ (where $\mathcal{V}^+$ is the shorthand notation for $\mathcal{V}[k+1]$). Consider the function

$$L := \Delta\mathcal{V} + \|\mathcal{C}_{\tilde{G}}\tilde{x}\|^2 - \gamma^2\|u_{lin}\| + 2\tilde{v}_{NL}^{\mathrm{T}}\mathcal{W}(\epsilon\bar{u}_{NL} - \tilde{v}_{NL}) < 0 \tag{A.1}$$

where the last term comes from consideration that $\mathrm{Dz} \in \mathrm{Sector}[0, \epsilon I]$ which implies that there exists a diagonal matrix $\mathcal{W} > 0$ such that $\mathrm{Dz}(\bar{u}_{NL})^{\mathrm{T}}\mathcal{W}(\epsilon\bar{u}_{NL} - \mathrm{Dz}(\bar{u}_{NL})) \geq 0$ [Khalil, 2002] and therefore $2\tilde{v}_{NL}^{\mathrm{T}}\mathrm{Dz}(\bar{u}_{NL})\mathcal{W}(\bar{u}_{NL} - \tilde{v}_{NL}) \geq 0$. Expanding (A.1) and substituting $\bar{u}_{NL} = u_{lin} - v_d$ gives

$$\begin{aligned} L = {} & \tilde{x}^{\mathrm{T}}\mathcal{C}_{\tilde{G}}^{\mathrm{T}}\mathcal{C}_{\tilde{G}}\tilde{x} - \gamma^2 u_{lin}^{\mathrm{T}}u_{lin} + \left(\tilde{x}^+\right)^{\mathrm{T}}\mathcal{P}\left(\tilde{x}^+\right) - \tilde{x}^{\mathrm{T}}\mathcal{P}\tilde{x} \\ & + 2\tilde{v}_{NL}^{\mathrm{T}}\epsilon\mathcal{W}u_{lin} - 2\tilde{v}_{NL}^{\mathrm{T}}\epsilon\mathcal{W}v_d - 2\tilde{v}_{NL}^{\mathrm{T}}\mathcal{W}\tilde{v}_{NL} \end{aligned} \tag{A.2}$$

where $\mathcal{P} = \mathcal{C}_{\tilde{G}}^{\mathrm{T}}\mathcal{C}_{\tilde{G}}$. Cross-product terms involving u_{lin} and $\tilde{v}_{NL}$ are grouped as follows

$$\begin{aligned} & -\left[\gamma^2 u_{lin}^{\mathrm{T}}u_{lin} - 2\tilde{v}_{NL}^{\mathrm{T}}\epsilon\mathcal{W}u_{lin}\right] = \\ & -\|\gamma u_{lin} - \gamma^{-1}\mathcal{W}\epsilon\tilde{v}_{NL}\|^2 + \gamma^{-2}\tilde{v}_{NL}^{\mathrm{T}}\epsilon^2\mathcal{W}^2\tilde{v}_{NL} \end{aligned} \tag{A.3}$$

Combining (A.3) with (A.2), and using $\tilde{x}^+$ from (15) and that $v_d = \mathcal{F}_{\tilde{G}}\tilde{x}$, and expanding $\tilde{x}^{+^{\mathrm{T}}}\mathcal{P}\tilde{x}^+ - \tilde{x}^{\mathrm{T}}\mathcal{P}\tilde{x}$ the following cost function is obtained

$$\begin{aligned} & L = \tilde{x}^{\mathrm{T}}\left(\mathcal{C}_{\tilde{G}}^{\mathrm{T}}\mathcal{C}_{\tilde{G}} + \mathcal{A}_{\tilde{G}}^{\mathrm{T}}\mathcal{P}\mathcal{A}_{\tilde{G}} + 2\mathcal{F}_{\tilde{G}}^{\mathrm{T}}\mathcal{B}_{\tilde{G}}^{\mathrm{T}}\mathcal{P}\mathcal{A}_{\tilde{G}} + \right. \\ & \left. \mathcal{F}_{\tilde{G}}^{\mathrm{T}}\mathcal{B}_{\tilde{G}}^{\mathrm{T}}\mathcal{P}\mathcal{B}_{\tilde{G}}\mathcal{F}_{\tilde{G}} - \mathcal{P}\right)\tilde{x} + \\ & 2\tilde{x}^{\mathrm{T}}\left(\mathcal{A}_{\tilde{G}}^{\mathrm{T}}\mathcal{P}\mathcal{B}_{\tilde{G}} + \mathcal{F}_{\tilde{G}}^{\mathrm{T}}\mathcal{B}_{\tilde{G}}^{\mathrm{T}}\mathcal{P}\mathcal{B}_{\tilde{G}} - \epsilon\mathcal{W}\mathcal{F}_{\tilde{G}}^{\mathrm{T}}\right)\tilde{v}_{NL} \\ & -\tilde{v}_{NL}^{\mathrm{T}}\left(2\mathcal{W} - \mathcal{B}_{\tilde{G}}^{\mathrm{T}}\mathcal{P}\mathcal{B}_{\tilde{G}} - \gamma^{-2}\epsilon^2\mathcal{W}^2\right)\tilde{v}_{NL} - \\ & \|\gamma u_{lin} - \gamma^{-1}\mathcal{W}\epsilon\tilde{v}_{NL}\|^2 \end{aligned} \tag{A.4}$$

The parameter $\mathcal{Z}$ can be defined as $\mathcal{Z} = 2\mathcal{W} - \mathcal{B}_{\tilde{G}}^{\mathrm{T}}\mathcal{P}\mathcal{B}_{\tilde{G}} - \gamma^{-2}\epsilon^2\mathcal{W}^2$ and the terms involving $\tilde{v}_{NL}$ and $\tilde{x}$ are grouped so that the new cost function becomes

$$\begin{aligned} & L = \tilde{x}^{\mathrm{T}}\left[\mathcal{C}_{\tilde{G}}^{\mathrm{T}}\mathcal{C}_{\tilde{G}} + \mathcal{A}_{\tilde{G}}^{\mathrm{T}}\mathcal{P}\mathcal{A}_{\tilde{G}} + 2\mathcal{F}_{\tilde{G}}^{\mathrm{T}}\mathcal{B}_{\tilde{G}}^{\mathrm{T}}\mathcal{P}\mathcal{A}_{\tilde{G}} + \right. \\ & \mathcal{F}_{\tilde{G}}^{\mathrm{T}}\mathcal{B}_{\tilde{G}}^{\mathrm{T}}\mathcal{P}\mathcal{B}_{\tilde{G}}\mathcal{F}_{\tilde{G}} - \mathcal{P} + \\ & \left(\mathcal{B}_{\tilde{G}}^{\mathrm{T}}\mathcal{P}\mathcal{A}_{\tilde{G}} + \mathcal{B}_{\tilde{G}}^{\mathrm{T}}\mathcal{P}\mathcal{B}_{\tilde{G}}\mathcal{F}_{\tilde{G}} - \epsilon\mathcal{W}\mathcal{F}_{\tilde{G}}\right)^{\mathrm{T}}\mathcal{Z}^{-1} \\ & \left.\left(\mathcal{B}_{\tilde{G}}^{\mathrm{T}}\mathcal{P}\mathcal{A}_{\tilde{G}} + \mathcal{B}_{\tilde{G}}^{\mathrm{T}}\mathcal{P}\mathcal{B}_{\tilde{G}}\mathcal{F}_{\tilde{G}} - \mathcal{W}\mathcal{F}_{\tilde{G}}\right)\right]\tilde{x} \\ & -\|\gamma u_{lin} - \gamma^{-1}\mathcal{W}\epsilon\tilde{v}_{NL}\|^2 \\ & -\|\mathcal{Z}^{\frac{1}{2}}\tilde{v}_{NL} - \mathcal{Z}^{-\frac{1}{2}}\left(\mathcal{B}_{\tilde{G}}^{\mathrm{T}}\mathcal{P}\mathcal{A}_{\tilde{G}} + \mathcal{B}_{\tilde{G}}^{\mathrm{T}}\mathcal{P}\mathcal{B}_{\tilde{G}}\mathcal{F}_{\tilde{G}} - \epsilon\mathcal{W}\mathcal{F}_{\tilde{G}}\right)\tilde{x}\|^2 \end{aligned} \tag{A.5}$$

The terms involving $\mathcal{F}_{\tilde{G}}$ and $\mathcal{F}_{\tilde{G}}^{\mathrm{T}}\mathcal{F}_{\tilde{G}}$ in the first term of (A.5) are grouped such that so that the cost function

becomes

$$\begin{aligned}
&L = L_a + L_b + L_c \\
&L_a = \tilde{x}^{\mathrm{T}} \left(\mathcal{C}_{\tilde{G}}^{\mathrm{T}}\mathcal{C}_{\tilde{G}} + \mathcal{A}_{\tilde{G}}^{\mathrm{T}}\mathcal{P}\mathcal{A}_{\tilde{G}} - \mathcal{P} + \mathcal{A}_{\tilde{G}}^{\mathrm{T}}\mathcal{P}\mathcal{B}_{\tilde{G}}\mathcal{Z}^{-1}\right. \\
&\mathcal{A}_{\tilde{G}}\mathcal{P}\mathcal{B}_{\tilde{G}}^{\mathrm{T}} - \mathcal{A}_{\tilde{G}}^{\mathrm{T}}\mathcal{P}\mathcal{B}_{\tilde{G}}\left(\mathcal{Z}\epsilon^{-1}\mathcal{W}^{-1} - I\right)^{\mathrm{T}}\mathcal{Z}^{-1} \\
&\left(\mathcal{Z}\epsilon^{-1}\mathcal{W}^{-1} - I\right)\mathcal{B}_{\tilde{G}}^{\mathrm{T}}\mathcal{P}\mathcal{A}_{\tilde{G}} \\
&\left. - \mathcal{A}'_{\tilde{G}}\mathcal{P}\mathcal{B}_{\tilde{G}}\mathcal{B}_{\tilde{G}}^{\mathrm{T}}\mathcal{P}\mathcal{A}_{\tilde{G}}\right)\tilde{x} \\
&= \tilde{x}^{\mathrm{T}}\left(\mathcal{A}_{\tilde{G}}^{\mathrm{T}}\mathcal{P}\mathcal{A}_{\tilde{G}} - \mathcal{P} + \mathcal{C}_{\tilde{G}}^{\mathrm{T}}\mathcal{C}_{\tilde{G}} + \mathcal{A}_{\tilde{G}}^{\mathrm{T}}\mathcal{P}\mathcal{B}_{\tilde{G}}\right. \\
&\left.\left[\mathcal{Z}^{-1} - (\mathcal{Z}\epsilon^{-1}\mathcal{W}^{-1})\mathcal{Z}^{-1}(\mathcal{Z}\epsilon^{-1}\mathcal{W}^{-1}) - I\right]\mathcal{B}_{\tilde{G}}^{\mathrm{T}}\mathcal{P}\mathcal{A}_{\tilde{G}}\right)\tilde{x} \\
&= \tilde{x}^{\mathrm{T}}\left(\mathcal{A}_{\tilde{G}}^{\mathrm{T}}\mathcal{P}\mathcal{A}_{\tilde{G}} - \mathcal{P} + \mathcal{C}_{\tilde{G}}^{\mathrm{T}}\mathcal{C}_{\tilde{G}} - \mathcal{A}_{\tilde{G}}^{\mathrm{T}}\mathcal{P}\mathcal{B}_{\tilde{G}}\right. \\
&\left.\left[\epsilon^{-2}\mathcal{W}^{-2}\mathcal{Z} - 2\epsilon^{-1}\mathcal{W}^{-1} + I\right]\mathcal{B}_{\tilde{G}}^{\mathrm{T}}\mathcal{P}\mathcal{A}_{\tilde{G}}\right)\tilde{x} \\
&L_b = \|\mathcal{Z}^{\frac{1}{2}}\left(\epsilon\mathcal{W}\mathcal{F}_{\tilde{G}} + \left(\mathcal{Z}\epsilon^{-1}\mathcal{W}^{-1} - I\right)\mathcal{B}_{\tilde{G}}^{\mathrm{T}}\mathcal{P}\mathcal{A}_{\tilde{G}}\right)\tilde{x}\|^2 \\
&+\|\mathcal{Z}^{-\frac{1}{2}}\left(\mathcal{B}_{\tilde{G}}^{\mathrm{T}}\mathcal{P}\mathcal{B}_{\tilde{G}}\mathcal{F}_{\tilde{G}} + \mathcal{B}_{\tilde{G}}^{\mathrm{T}}\mathcal{P}\mathcal{A}_{\tilde{G}}\right)\tilde{x}\|^2 + \mathcal{B}_{\tilde{G}}^{\mathrm{T}}\mathcal{P}\mathcal{B}_{\tilde{G}}\|\mathcal{F}_{\tilde{G}}\tilde{x}\|^2 \\
&L_c = -\|\mathcal{Z}^{\frac{1}{2}}\tilde{v}_{NL} - \mathcal{Z}^{-\frac{1}{2}}\left(\mathcal{B}_{\tilde{G}}^{\mathrm{T}}\mathcal{P}\mathcal{A}_{\tilde{G}} + \mathcal{B}_{\tilde{G}}^{\mathrm{T}}\mathcal{P}\mathcal{B}_{\tilde{G}}\mathcal{F}_{\tilde{G}}\right. \\
&\left.-\epsilon\mathcal{W}\mathcal{F}_{\tilde{G}}\right)\tilde{x}\|^2 - \|\gamma u_{lin} - \gamma^{-1}\mathcal{W}\epsilon\tilde{v}_{NL}\|^2
\end{aligned} \tag{A.6}$$

The last term, L_c in (A.6) is a negative quadratic term, therefore if L_b and L_c can be set to 0, then $L < 0$. Setting $L_b = 0$ and noting that $Z > 0$ yields $\mathcal{F}_{\tilde{G}}$ defined by

$$-\left(\frac{(2-\epsilon)\mathcal{W}^{-1}}{\epsilon^2} - \gamma^{-2}I - \epsilon^{-2}\mathcal{W}^{-2}\mathcal{B}_{\tilde{G}}^{\mathrm{T}}\mathcal{P}\mathcal{B}_{\tilde{G}}\right)\mathcal{B}_{\tilde{G}}{}^{\mathrm{T}}\mathcal{P}\mathcal{A}_{\tilde{G}} \tag{A.7}$$

where $\mathcal{P} = \mathcal{P}^{\mathrm{T}} > 0$ comes from solving the Riccati equation which makes $L_a = 0$ i.e.

$$\begin{aligned}
&\mathcal{A}_{\tilde{G}}^{\mathrm{T}}\mathcal{P}\mathcal{A}_{\tilde{G}} - \mathcal{P} + \mathcal{C}_{\tilde{G}}^{\mathrm{T}}\mathcal{C}_{\tilde{G}} - \\
&\mathcal{A}_{\tilde{G}}^{\mathrm{T}}\mathcal{P}\mathcal{B}_{\tilde{G}}\left[\epsilon^{-2}\mathcal{W}^{-2}\mathcal{Z} - 2\epsilon^{-1}\mathcal{W}^{-1} + I\right]\mathcal{B}_{\tilde{G}}^{\mathrm{T}}\mathcal{P}\mathcal{A}_{\tilde{G}}
\end{aligned} \tag{A.8}$$

□

B Proof of Lemma 1

Proof For the rate limiter with filter $\rho(z^{-1})$ connected to the output, $v_{NL} = \mathrm{sat}(k_r(u_n - v_n))$ and $w_n = \rho(z^{-1})\frac{k_r T_s z^{-1}}{1-z^{-1}}v_{NL}$ (where u is the shorthand notation for $u[k]$). Substituting for k_r and $\rho(z^{-1})$ gives

$$w_n(1 - z^{-1}) = T_s\mathrm{sat}(k_r(u_n - v_n)) \tag{B.1}$$

Since $w_n = \rho(z^{-1})v_n$ then $w_n - v_n = T_s\mathrm{sat}(k_r(u_n - v_n))$. Proving an upper bound, γ_φ, on the system $u_n \to w_n$ is equivalent to proving the IQC of the form

$$\begin{aligned}
0 \leq&\gamma_\varphi^2\|u_n\|^2 - \|w_n\|^2 \\
=&\gamma_\varphi^2\|v_n + (u_n - v_n)\|^2 - \|v_n + (w_n - v_n)\|^2
\end{aligned} \tag{B.2}$$

which refers to

$$\begin{bmatrix} v_n^{\mathrm{T}} & (u_n - v_n)^{\mathrm{T}} & (w_n - v_n)^{\mathrm{T}} \end{bmatrix}\Gamma_\varphi\begin{bmatrix} v_n^{\mathrm{T}} \\ (u_n - v_n)^{\mathrm{T}} \\ (w_n - v_n)^{\mathrm{T}} \end{bmatrix} \tag{B.3}$$

giving $\Gamma_{\varphi_{11}} = \gamma_\varphi^2 - 1$, $\Gamma_{\varphi_{12}} = \Gamma_{\varphi_{21}} = \Gamma_{\varphi_{22}} = \gamma_\varphi^2$, $\Gamma_{\varphi_{13}} = \Gamma_{\varphi_{31}} = \Gamma_{\varphi_{33}} = -1$, $\Gamma_{\varphi_{23}} = \Gamma_{\varphi_{32}} = 0$. For inequality (B.2) to hold, the following inequalities must hold [Megretski, 2001]

$$\begin{bmatrix} \Gamma_{\varphi_{11}} & \Gamma_{\varphi_{12}} \\ \Gamma_{\varphi_{21}} & 2\Gamma_{\varphi_{22}} \end{bmatrix} \geq 0, \qquad \Gamma_{\varphi_{22}} + 2\kappa\Gamma_{\varphi_{23}} + \kappa^2\Gamma_{\varphi_{33}} \geq 0 \tag{B.4}$$

The first inequality in (B.4) yields $\gamma_\varphi^2 \geq 2$ while the second gives $\gamma_\varphi^2 \geq \kappa^2$ which results in the upper bound $\gamma_\varphi = \max\{\kappa, \sqrt{2}\}$. □

References

P.J. Campo and M. Morari. Robust control of processes subject to saturation nonlinearities. *Computers & Chemical Engineering*, 14(45):343–358, 1990.

A. Chakraborty, P. Seiler, and G. J. Balas. Local performance analysis of uncertain polynomial systems with applications to actuator saturation. In *IEEE Conference on Decision and Control and European Control Conference*, pages 8176–8181, Orlando, FL, 2011.

K. W. Corscadden and S. R. Duncan. Multivariable disturbance modelling for web processes. *International Journal of Systems Science*, 31(1):97–106, 2000.

S. R. Duncan. The design of a fast orbit beam stabilisation system for the Diamond synchrotron. Technical Report 2296/07, Department of Engineering Science, University of Oxford, UK, 2007.

S. R. Duncan and G. F. Bryant. The spatial bandwidth of cross-directional control systems for web processes. *Automatica*, 33(2):139–153, 1997.

L. El Ghaoui and S. I. Niculescu, editors. *Advances in Linear Matrix Inequality Methods in Control: Advances in Design and Control*. Society for Industrial and Applied Mathematics, Philadelphia, PA, 2000.

A. P. Featherstone, J. G. VanAntwerp, and R. D. Braatz. *Identification and Control of Sheet and Film Processes*. Springer, 2000.

S. Gayadeen. *Synchrotron Electron Beam Control*. PhD thesis, Department of Engineering Science, University of Oxford, UK, 2014.

S. Gayadeen and S. R. Duncan. Uncertainty modeling and robust stability analysis of a synchrotron electron beam stabilisation control system. In *IEEE 51st Annual Conference on Decision and Control*, pages 931–936, Maui, HI, 2012.

S. Gayadeen and S. R. Duncan. Anti-windup compensation for electron beam stabilisation control systems on synchrotrons with rate constrained actuators. In *European Control Conference*, pages 2752–2757, Zürich, Switzerland, 2013.

S. Gayadeen and S. R. Duncan. Design of an electron beam stabilisation controller for a synchrotron. *Control Engineering Practice*, 26:201–210, 2014.

S. Gayadeen, S. R. Duncan, C. Christou, M. T. Heron, and J. Rowland. Diamond Light Source Booster fast orbit feedback system. In *International Conference on Accelerator and Large Experimental Physics Control Systems*, pages 160–163, Grenoble, France, 2011.

G. C. Goodwin, S. E. Graebe, and W. S. Levine. Internal model control of linear systems with saturating actuators. In *Proceedings of the European Control Conference*, pages 1072–1077, Groningen, Netherlands, 1993.

W. P. Heath. Orthogonal functions for cross-directional control of web forming processes. *Automatica*, 32(2): 183–198, 1996.

U. Jonsson. Lecture notes on Integral Quadratic Constraints. Available at: `http://www.montefiore.ulg.ac.be/services/systems/grad04/lecturenotes.pdf`, 2001.

H. K. Khalil, editor. *Nonlinear Systems*. Prentice Hall, Upper Saddle River, NJ, 2002.

A. Megretski. New IQC for quasi-concave nonlinearities. *International Journal of Robust and Nonlinear Control*, 11(7):603–620, 2001.

A. Megretski and A. Rantzer. System analysis via Integral Quadratic Constraints. *IEEE Transactions on Automatic Control*, 42(6):819–830, 1997.

R. M. Morales and W. P. Heath. The robustness and design of constrained cross-directional control via Integral Quadratic Constraints. *IEEE Transactions on Control Systems Technology*, 19(6):1421–1432, 2011.

R. M. Morales, G. Li, and W. P. Heath. Anti-windup and the preservation of robustness against structured norm-bounded uncertainty. *International Journal of Robust and Nonlinear Control*, 2013.

M. Morari and E. Zafiriou. *Robust Process Control*. Prentice-Hall, Englewood Cliffs, NJ, 1989.

E. F. Mulder, M. V. Kothare, and M. Morari. Multivariable anti-windup controller synthesis using linear matrix inequalities. *Automatica*, 37(9):1407 – 1416, 2001.

A. Rantzer. On the Kalman Yakubovich Popov lemma. *Systems & Control Letters*, 28(1):7–10, 1996.

J. Rowland, M. G. Abbott, J. A. Dobbing, M. T. Heron, I. Martin, G. Rehm, and I. Uzun. Status of the Diamond fast orbit feedback system. In *International Conference on Accelerator and Large Experimental Physics Control Systems*, pages 535–537, Knoxville, Tennessee, 2007.

J. Sofrony, M. C. Turner, and I. Postlethwaite. Anti-windup synthesis for systems with rate-limits using Riccati equations. *International Journal of Control*, 83(2):233–245, 2010.

M. C. Turner, G. Herrmann, and I. Postlethwaite. Discrete time antiwind-up - part 1: Stability and performance. In *European Control Conference*, Cambridge, UK, 2003.

P. F Weston and I. Postlethwaite. Linear conditioning for systems containing saturating actuators. *Automatica*, 36(9):1347 – 1354, 2000.

A. Zheng, M. V. Kothare, and M. Morari. Anti-windup design for internal model control. *International Journal of Control*, 60(5):1015–1024, 1993.